Subthreshold and suprathreshold vibrational resonance in the FitzHugh-Nagumo neuron model

Jinjie Zhu,* Chen Kong, and Xianbin Liu†
State Key Laboratory of Mechanics and Control of Mechanical Structures, College of Aerospace Engineering, Nanjing University of Aeronautics and Astronautics, Nanjing 210016, China
(Received 11 May 2016; revised manuscript received 10 July 2016; published 8 September 2016)

We study the subthreshold and suprathreshold vibrational resonance in the FitzHugh-Nagumo neuron model. For the subthreshold situation, two cases where the stationary states are equilibrium point and limit cycle are considered, where different natures of vibrational resonance are observed via theoretical and numerical methods. Especially when the frequency of the high-frequency driving force is near the so-called canard-resonance frequency, the firing rate can be significantly enhanced at the presence of noise. For the suprathreshold situation, we show that the local maxima of the response amplitude are located at the transition boundaries of different phase-locking patterns. The minimal required forcing amplitudes of high-frequency signal of the firing onset are just multiples of the spiking frequency. Furthermore, phase portraits and time series show that the presence of the global maxima of the response results from not only the suprathreshold but also the subthreshold phase-locking modes. In spite of the distinct characteristics for two stationary states on subthreshold oscillation, the suprathreshold vibrational resonance showed no qualitative difference between the two cases.

DOI: 10.1103/PhysRevE.94.032208

I. INTRODUCTION

Stochastic resonance (SR) has engaged much attention since it was first proposed by Benzi *et al.* [1]. Due to its counterintuitive features and potential applications, SR has been investigated in optical systems, electronic and magnetic systems, neuronal systems, etc. [2]. It shows that there exists an optimal strength of noise so that the transmission of the weak signal in a nonlinear system could be enhanced. Because of the random nature of noise, researchers have been looking for other alternatives to produce similar SR behaviors, e.g., rectangular pulse trains [3] or suitable chaotic signals [4]. Among these alternatives, high-frequency signal (HFS), compared with the weak low-frequency signal (LFS), is of great interest to many researchers since bichromatic signals are very important in many fields, e.g., acoustics, laser physics, engineering, and neuroscience [5]. The resonant amplification of the signal output induced by HFS was first named vibrational resonance (VR) by Landa and McClintock [6]. Since then, VR has been studied theoretically, numerically, and experimentally in many systems [5,7–12].

In excitable neuronal systems, information transmission is vital and VR seems to be an efficient way to improve its transport. In this paper, we investigate VR in the FitzHugh-Nagumo (FHN) neuron model [13]. It is a simple but paradigmatic model for establishing neuron activities, and is defined as follows [7,12]:

$$\begin{aligned} \varepsilon\dot{x} &= x - \tfrac{1}{3}x^3 - y, \\ \dot{y} &= x + a + A\cos(\omega t) + B\cos(\Omega t), \end{aligned} \tag{1}$$

where x and y represent the fast membrane potential variable and the slow variable related to the conductivity of the potassium channels, respectively. ε is the time separation parameter. Without external inputs, a is a bifurcation parameter so that for $a > 1$, the system will have only one equilibrium point (x_*, y_*), where $x_* = -a$, $y_* = \frac{a^3}{3} - a$. For a slightly smaller than 1, the system will undergo a supercritical Hopf bifurcation, so a small limit cycle will emerge. Most studies on VR of the FHN model ignored the subthreshold oscillation, where VR is realized by the periodic modulation of LFS; i.e., for one half period of LFS, the neurons spike most, while for the other half, they spike least. However, subthreshold oscillations have been observed *in vivo* [14,15] and *in vitro* [16,17]. It was shown that afferent discharge generated ectopically in the cell soma of dorsal root ganglion (DRG) neurons is critically dependent on subthreshold membrane potential oscillations [15]. Moreover, it was proved that subthreshold oscillations could influence the firing behaviors in theoretical neuron models [18–21]. Thus, it is worth investigating its roles in VR.

For the suprathreshold case, when the input of HFS induces spikes, VR has been extensively investigated in excitable systems due to its unambiguous manifestation whether theoretically [7] or numerically and experimentally [12]. A single peak which is analogous to the SR case is characterized by the response amplitude Q. Moreover, it has been shown that multiple VR can be induced by time delayed feedback in overdamped uncoupled and coupled bistable systems and in Duffing oscillators [10,22,23]. As for excitable systems, especially for the FHN model, similar multiple VR has been obtained by constant and time-varying delay [24,25]. Previous studies were mostly devoted to the single parameter of HFS, mainly to the amplitude. Global views on both amplitude and frequency of HFS of VR have begun to be noticed in Refs. [8,9]. Yang *et al.* [8] provided a global view by tuning both amplitude and frequency of HFS to find the relation between the different phase-locking modes and VR, which shows each maximum of response is exactly located at the transition boundary of phase patterns. As the bichromatic signals are added in the fast variable in their paper, we want to check whether these results are true when the bichromatic signals are added in the slow variable.

We fix $\varepsilon = 0.1$ throughout this paper so that subthreshold oscillation survives under small perturbations. $A\cos(\omega t)$ and $B\cos(\Omega t)$ are LFS and HFS, respectively. $A = 0.005$ was

*jinjiezhu@nuaa.edu.cn
†xbliu@nuaa.edu.cn

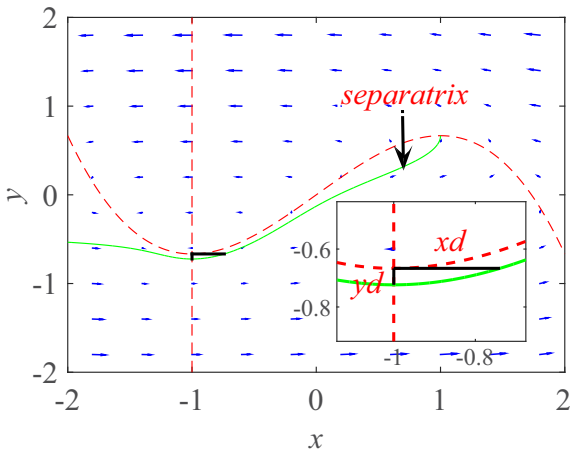

FIG. 1. The phase portrait of the FHN neuron model. The red dashed lines are nullclines and the green line is the separatrix by numerical integration. Any initial point under the separatrix undergoes a large excursion (spike) and terminates around the equilibrium point. Blue arrows represent the vector field. Inset: the local magnification of the intersection between the nullclines, where xd and yd represent the distance between the separatrix and the equilibrium point ($a > 1$) or the limit cycle ($a < 1$) along the x and y directions, respectively (bold black lines).

set for weak LFS and $\omega \ll \Omega$ was assumed. The phase portrait of the FHN neuron model is illustrated in Fig. 1. In the following, both the subthreshold and suprathreshold VR will be investigated. This paper is organized as follows: The subthreshold VR will be studied in Sec. II where two cases of resting state, equilibrium point ($a > 1$) and limit cycle ($a < 1$), are investigated separately. The suprathreshold VR will be investigated in Sec. III. Finally, some conclusions and discussions are given in Sec. IV.

II. SUBTHRESHOLD VIBRATIONAL RESONANCE

For the subthreshold vibrational resonance, we fix $\omega = 0.1$. Two separate cases, i.e., $a > 1$ and $a < 1$, are studied since they have different stationary states (equilibrium state and limit cycle oscillation).

A. Case 1. $a > 1$

We choose $a = 1.01$. The system will have only one equilibrium point. Since we consider the subthreshold vibrational resonance, B is settled small enough as there is no spike when HFS is added. In this case, we separate the slow and fast motion by [11]

$$x(t) = X(t) + \psi(t,\tau), \tag{2}$$

where $X(t)$ is the slow motion and $\psi(t,\tau)$ is the fast motion of the 2π period of fast time $\tau = \Omega t$, and the mean value of $\psi(t,\tau)$ with respect to τ is

$$\bar{\psi} = \frac{1}{2\pi}\int_0^{2\pi} \psi(t,\tau)d\tau = 0. \tag{3}$$

First, we eliminate variable y in Eq. (1) by some simple calculations:

$$\varepsilon\ddot{x} = (1-x^2)\dot{x} - x - a - A\cos(\omega t) - B\cos(\Omega t). \tag{4}$$

Substituting Eqs. (2) and (3) into Eq. (4), and separating the slow and fast motion, we obtain

$$\varepsilon\ddot{\tilde{X}} + [(\tilde{X}-a)^2 + \overline{\psi^2} - 1]\dot{\tilde{X}} + \tilde{X} = -A\cos(\omega t), \tag{5a}$$

$$\varepsilon\ddot{\psi} + [(X+\psi)^2 - 1]\dot{\psi} + (\psi^2 - \overline{\psi^2})\dot{X} + (1+2X\dot{X})\psi = -B\cos(\Omega t), \tag{5b}$$

where we have used $\tilde{X} = X - x_*$ [(x_*, y_*) is the stable equilibrium point] and $\int_0^{2\pi} f(\psi)\frac{\partial\psi}{\partial t}d\tau = \int_0^{2\pi} f(\psi)\Omega\frac{\partial\psi}{\partial\tau}d\tau = \int_0^{2\pi} f(\psi)\Omega d\psi = 0$ in Eq. (5a). $f(\psi)$ is ψ or ψ^2. Assuming $\Omega \gg 1$, we have $\ddot{\psi} \gg \dot{\psi}, \psi, \psi^2$, and according to $X \approx -1$ (because A is small enough and a is very close to 1), we can simplify Eq. (5b) as

$$\varepsilon\ddot{\psi} = -B\cos(\Omega t). \tag{6}$$

The solution to Eq. (6) is $\psi = \frac{B}{\varepsilon\Omega^2}\cos(\Omega t)$; thus we have

$$\overline{\psi^2} = \frac{B^2}{2\varepsilon^2\Omega^4}, \tag{7}$$

and Eq. (5a) turns to

$$\ddot{\tilde{X}} + d\dot{\tilde{X}} + \frac{1}{\varepsilon}\tilde{X} = -\frac{A\cos(\omega t)}{\varepsilon}, \tag{8}$$

where $d = \frac{1}{\varepsilon}[\frac{B^2}{2\varepsilon^2\Omega^4} - 1 + (a-\tilde{X})^2]$. Due to the nonlinear damping term d in Eq. (8), direct solution is hopeless. Instead, we use the following approximation. $A = 0.005$, which is much smaller than ε, so that in the limit $t \to \infty$ we have $A_{\tilde{X}} = \frac{A}{\varepsilon\sqrt{(\omega_r{}^2-\omega^2)^2+d^2\omega^2}} < \frac{A}{\varepsilon(\omega_r{}^2-\omega^2)} \approx 5\times10^{-3}$, where $A_{\tilde{X}}$ is the amplitude of $\tilde{X}$ (we will see later that $A_{\tilde{X}} \approx 5.5\times10^{-3}$) and $\omega_r = \sqrt{\varepsilon^{-1}}$, which corresponds to the subthreshold oscillation frequency or the so-called canard-resonance frequency [18]. Thus, $d > 0$ for all values of B and Ω. We omit $\tilde{X}$ in d, so Q can be approximated as

$$Q = \frac{A}{\varepsilon\sqrt{\left(\omega_r^2-\omega^2\right)^2 + \hat{d}^2\omega^2}}, \tag{9}$$

where $\hat{d} = \frac{1}{\varepsilon}(\frac{B^2}{2\varepsilon^2\Omega^4} - 1 + a^2)$. Let

$$S = \left(\omega_r^2-\omega^2\right)^2 + \hat{d}^2\omega^2. \tag{10}$$

Then we can calculate the minimum and maximum of Q which correspond to the maximum and minimum of S, respectively. For fixed Ω, S is a function of B. The extremum of S is obtained by calculating $S_B = 2\hat{d}\hat{d}_B\omega^2 = 0$. According to $S_{BB} = 2\hat{d}_B^2\omega^2 + 2\hat{d}\hat{d}_{BB}\omega^2 > 0$, the only maximum of Q is when $B = 0$. We can verify it by computing Q numerically which is given by [18] $Q = \sqrt{Q_{\sin}{}^2 + Q_{\cos}{}^2}$, where

$$Q_{\sin} = \frac{\omega}{2\pi n}\int_0^{\frac{2\pi n}{\omega}} 2x(t)\sin(\omega t)dt,$$
$$Q_{\cos} = \frac{\omega}{2\pi n}\int_0^{\frac{2\pi n}{\omega}} 2x(t)\cos(\omega t)dt. \tag{11}$$

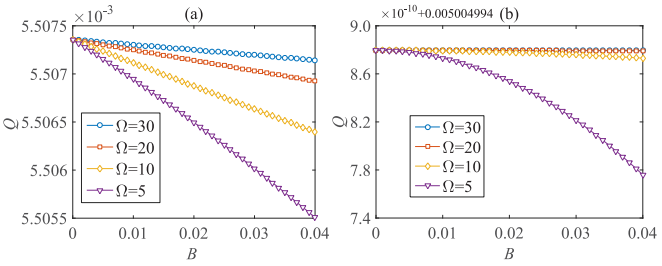

FIG. 2. Response amplitude Q versus HFS amplitude B for different HFS frequencies Ω. (a) Numerical results. (b) Theoretical results for Eq. (9). Parameters: $a = 1.01$, $A = 0.005$, $\omega = 0.1$. Note that the range of response for theoretical results is much smaller than that for numerical simulation.

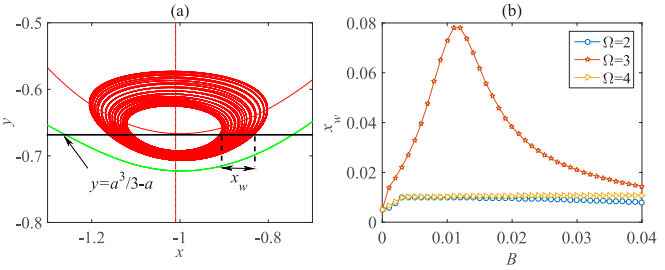

FIG. 4. (a) Phase portrait of Eq. (1). x_w denotes the width of orbit at $y = \frac{a^3}{3} - a$. Please note the asymmetry along the y direction. Parameters: $a = 1.01$, $\Omega = 3$, $B = 0.011$. (b) Variation in width of the orbit, x_w, as a function of B for different HFS frequencies Ω.

The Heun method is used to integrate Eq. (1) with time step 10^{-3}, $n = 100$, and ten period times of LFS are discarded as transients. The results are illustrated in Fig. 2(a). We can see that the addition of HFS decreases the transmission of LFS and this decreasing phenomenon is enhanced when the amplitude of HFS increases. The value and the change of Q are tiny while the rate of change becomes larger when Ω decreases. The theoretical results [Eq. (9)] underestimate the numerical results [the deviation mainly stems from the simplification of Eq. (5b)] but the changes are qualitatively the same [see Fig. 2(b)].

Note that for the above discussion, we have assumed $\Omega \gg 1$. The changes of Q-B curves seem to be monotonic for decreasing Ω. It is still unknown whether this kind of monotonicity will persist when Ω is not assumed large enough, especially when it is near the subthreshold frequency $\omega_r = \sqrt{\varepsilon^{-1}}$. Accordingly, the response amplitude Q is calculated versus three different frequencies of HFS as in Fig. 3(a). We can see from Fig. 3(a) that the monotonicity as in Fig. 2 no longer persists due to the resonance between HFS and canard oscillation. When the frequency of HFS is far from the canard frequency (either below or over), the response Q seems to change slowly as discussed above. When the frequency of HFS is near the canard frequency, at first, the increase of B will enhance response amplitude Q and after some critical value of B, it will drop to an even deeper value than that for frequencies not close to the canard frequency which represents a suppression of response to LFS. The profile of Fig. 3 for $\Omega = 3$ resembles the classical vibrational resonance curve. There is a single peak at $B = 0.011$ which shows the enhancement of the response amplitude by HFS. It should be noted that after the resonance, the increasing energy of the HFS input seems not to influence the response to the LFS (flatter curve after around $B = 0.025$). The mechanism for the subthreshold vibrational resonance could be explained as follows. Each orbit circled around the fixed point (x_*, y_*) has a frequency associated with the radius of the orbit. The nearer the orbit to the fixed point, the larger the frequency of the orbit (the frequency approaches ω_r when the orbit approaches the fixed point). There is an optimal amplitude of HFS whereby the orbit will be pulled to the radius where the frequency of the orbit matches the frequency of HFS. In that case, the resonance happens and the response to the LFS input will be mostly enhanced. So for HFS with a smaller frequency, the peak of Q will emerge at a larger amplitude [see Fig. 3(b)]. To ensure the presence of the peak, the frequency has a narrow range in that for a too small frequency of HFS, the optimal amplitude of HFS may already induce spikes which will be contrary to our purpose here to study the subthreshold VR and for a too large one there would be no resonant amplitude B as is illustrated in Fig. 2 (the only maximum should be $B = 0$). The flatter parts of the curves in Fig. 3(b) showed the orbits were pulled away from the resonant area and that the response amplitude of LFS was not affected by the amplitude change of HFS.

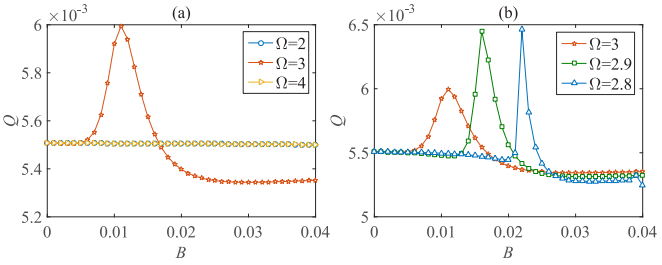

FIG. 3. Response amplitude Q versus HFS amplitude B for different frequencies Ω. Other parameters are the same as in Fig. 2.

We verify our result in a more intuitive and convenient way by the width of the orbit of x [11], denoted as x_w [the definition of x_w is clarified in Fig. 4(a)]. We choose the width of orbit at $y = \frac{a^3}{3} - a$ because the orbit circled around the fixed point (x_*, y_*); therefore the definition of x_w could always be meaningful. The results are illustrated in Fig. 4(b) (in fact, the width of the orbit of y is also applicable here). From Fig. 4(b), we can see the curves are qualitatively the same as Fig. 3(a). The peak at $B = 0.011$ showed that the width of the orbit defined in Fig. 4(a) reached the maximum as a signature of the vibration resonance.

More details can be revealed by the phase portraits of Eq. (1). As in Fig. 5, generally, with the increase of B, the radius of the trajectories will increase. For Ω away from the canard frequency ($\Omega = 2$, 4), the radius is much smaller than that for Ω near the canard frequency ($\Omega = 3$). For $\Omega = 3$, the optimal amplitude of HFS is at $B = 0.011$, where the difference between the inner and outer radius is maximized which corresponds to the previously calculated orbit width in Fig. 4. Further increasing the amplitude of HFS expands both the inner and outer radius. However, the inner radius increases

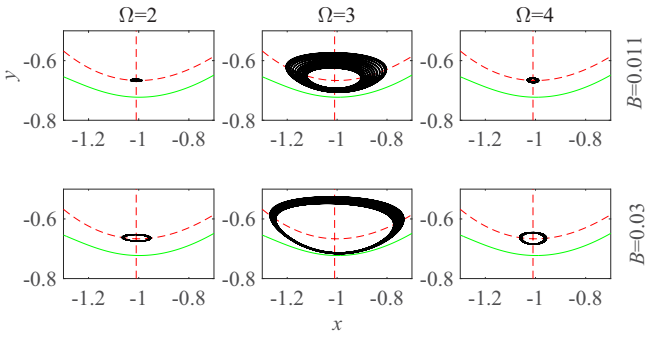

FIG. 5. Phase portraits of Eq. (1). From top to bottom: $B = 0.011$ and 0.03. From left to right: $\Omega = 2$, 3,4. Other parameters are the same as in Fig. 3.

faster than the outer radius which accounts for the decrease of the orbit width, thus decreasing the response amplitude to the LFS.

B. Case 2. $a < 1$

We choose $a = 0.998$ (slightly after Hopf bifurcation). In this case, without external input, the stationary state is limit cycle oscillation instead of equilibrium point. The situation becomes complicated when LFS and HFS are inputted at the presence of this limit cycle. We numerically calculated response amplitude Q. The results are in Fig. 6. We can see in this case the response amplitude Q is totally different from the previous case.

For Ω large enough [see Fig. 6(a)], initially, Q will increase with the increasing amplitude of HFS and after a critical value of B is exceeded, it begins to decrease. The transition point occurs at smaller B for smaller Ω. The periodiclike changes of Q indicate periodiclike enhancement and attenuation of the response to LFS. The general trend is that Q decreases as the increase of B along with the periodiclike changes (e.g., $\Omega = 5$) and the decreasing rate increases with decreasing Ω. It is interesting to see that this trend resembles the former case.

For Ω near the canard-resonance frequency, in addition to the obvious common characteristics, we can see that the profiles of Figs. 3(a) and 6(b) have two different features. First, for $a = 1.01$, there is only one peak ($B = 0.011$), while for $a = 0.998$, there are two adjacent peaks ($B = 0.006$ and $B = 0.008$). Second, the difference between the maximum and minimum of Q for the latter is more significant than the former.

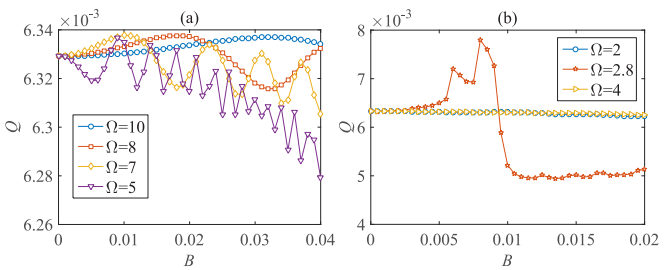

FIG. 6. Response amplitude Q versus HFS amplitude B for different frequencies Ω. Parameters: $a = 0.998$, $A = 0.005$, $\omega = 0.1$.

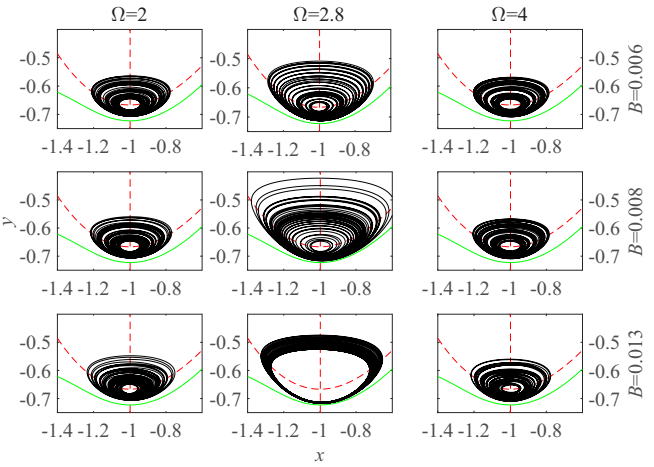

FIG. 7. Phase portraits of Eq. (1). From top to bottom: $B = 0.006$, 0.008, and 0.013. From left to right: $\Omega = 2$, 2.8,4. Other parameters are the same as in Fig. 6.

We conclude these two features are related to the presence of the limit cycle.

Again, we numerically calculate the phase portraits of Eq. (1) for $a = 0.998$. As is in Fig. 7, the radius seems to be unchanged for $\Omega = 2$, 4. When $\Omega = 2.8$, resonances happen for $B = 0.006$ and 0.008, which is in accordance with Fig. 6(b). The sudden decrease in Fig. 6(b) after $B = 0.008$ is induced by simultaneously decreasing the outer radius and increasing the inner radius, compared with the relative mild decrease in Fig. 3(a) where the outer radius always increases by increasing B.

What does subthreshold VR mean to neurons?

Although in neuronal systems, only the spikes themselves are important for the information transport, we can see that subthreshold VR may assist the neurons to fire. As noise is ubiquitous in neurons [26], additive Gaussian white noise $\xi(t)$ is added into Eq. (1) as

$$\begin{aligned} \varepsilon\dot{x} &= x - \tfrac{1}{3}x^3 - y, \\ \dot{y} &= x + a + A\cos(\omega t) + B\cos(\Omega t) + \sqrt{D}\xi(t), \end{aligned} \tag{12}$$

where $\langle\xi(t)\rangle = 0$, $\langle\xi(t)\xi(\tau)\rangle = D\delta(t-\tau)$. D is the strength of the noise. We calculate the average firing rate r_0 defined as [26]

$$r_0 = \frac{S_c(NT)}{NT}, \tag{13}$$

which denotes the mean number of spikes per unit time. $S_c(\cdot)$ is the spike count which calculates the number of spikes in the time window $(0, NT)$; T is the period of LFS; $N = 100$ and ten period times are discarded as transients. The results are in Fig. 8. The typical bell-shaped forms can be observed for both $a = 0.998$ and 1.01. The peaks show the resonances between HFS and the subthreshold oscillation. The firing rate is much higher for $a = 0.998$ than for $a = 1.01$. The reason can be explained by the decrease of xd or yd (see definition in Fig. 1) at the presence of the limit cycle in the case $a = 0.998$. Another phenomenon is that the resonant frequency is advanced for the limit cycle case. Therefore, it could be anticipated that subthreshold VR would also facilitate

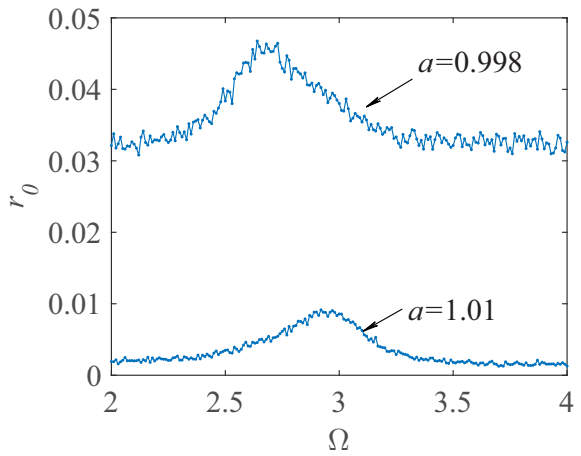

FIG. 8. Firing rate r_0 versus Ω. Parameters: $N = 100$, $D = 2 \times 10^{-4}$, $A = 0.005$, $\omega = 0.1$. For $a = 1.01$, $B = 0.011$; for $a = 0.998$, $B = 0.008$. The firing rate is obtained by averaging ten sample paths.

synchronization and propagation in neuron populations which will be our future work.

III. SUPRATHRESHOLD VIBRATIONAL RESONANCE

Continuing to increase the HFS amplitude will induce spikes. Vibration resonance happens when there is a value of HFS amplitude such that the neuron spikes most for one half period of LFS and least for the other half. However, further increasing of the amplitude could also produce VR. Yang *et al.* [8] proved these VRs are actually located at the transition boundaries of different phase-locking patterns (locking between the frequency of HFS and spikes). For their model, the bichromatic signals were added to the fast variable. As the signals are added into the slow variable in Eq. (1), we want to check if the mechanisms explained by Ref. [8] still hold.

We choose $a = 0.998$ as our example. In contrast to the former section, to get rid of the interference of the subthreshold oscillation, we adopt the measure Q_{th} in Eq. (11) (instead of Q) [18], where for $x(t) < x_{th}$, $x(t)$ is replaced by -1; for $x(t) \geqslant x_{th}$, $x(t)$ remains unchanged. x_{th} is set as 0. The range of the amplitude of HFS is [0, 0.4] which contains the subthreshold interval. Still, we use the Heun method to integrate Eq. (1). The results are illustrated in Fig. 9. It is found that the local maxima of response amplitude are still located at the transition boundaries of the phase-locking patterns as in Ref. [8]. Figure 10 illustrates the relations between VRs and phase-locking modes for a fixed amplitude ($B = 0.2$) and a fixed frequency ($\Omega = 3.4$) of HFS.

The minimal required forcing amplitude B of the firing onset is obtained at the forcing frequency about $\Omega = 2.5$ which is near the subthreshold frequency, as is still true compared with Ref. [8]. However, another local minimum of the firing onset exists at about $\Omega = 3.75$ which was not present in Ref. [8]. It can be numerically validated that the firing frequency is around 1.25; the two minima are just multiples of the firing frequency and their ratios correspond to the locking ratios (note that 2.5 is also close to the canard-resonance frequency which makes B the global minimum at $\Omega = 2.5$).

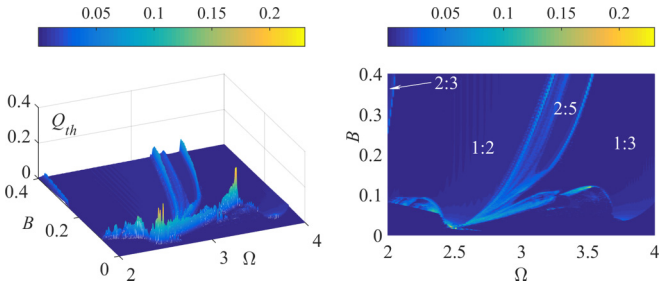

FIG. 9. Q_{th} versus B and Ω. Left: three-dimensional (3D) plot. Right: contour plot and phase-locking areas, where the locking ratio marked in white as m:n means m spikes per n cycles of HFS. Parameters: $a = 0.998$, $w = 0.251$, $A = 0.005$.

Thus, we can expect local minima at other multiples of 1.25, e.g., 1.25 at 1:1 phase-locking area. Coincidentally, the local minima in Ref. [8] coincide with the transition boundaries of phase patterns and the time separation ratio of theirs is $\varepsilon = 0.02$, much smaller than ours, along with the logarithmic form of coordinates, all of which covered up the phenomenon discussed here.

However, the local minimal required forcing amplitudes just predict the onset of firing but not the maxima of response amplitude. Clearly, two maxima of response amplitude Q_{th} can be seen in the left panel of Fig. 9. The first one is around $\Omega = 2.5$, which is close to the subthreshold frequency and the multiple of the firing frequency. The second one is around $\Omega = 3.5$, whereas it does not seem to correspond to any known frequency or its multiples. We take a deep look to investigate the mechanism by calculating the time series on these parameters (see Fig. 11). Phase-locking modes can be seen by comparing $x(t)$ and HFS on the firing state [1:2 for $\Omega = 2.5$ and 1:3 for $\Omega = 3.5$; see the dashed circles in Figs. 11(a) and 11(b)]. Besides, subthreshold oscillations also demonstrate phase-locking modes. For $\Omega = 2.5$, 1:1 subthreshold phase-locking is found, since Ω is near the resonance frequency (m:n subthreshold phase locking is defined as m large subthreshold oscillations per n cycles of HFS; accordingly,

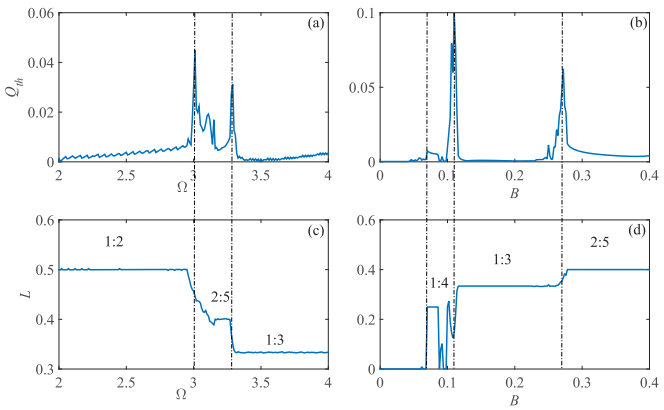

FIG. 10. Relations between VRs and phase-locking modes for a fixed amplitude and a fixed frequency of HFS. (a,c): $B = 0.2$; (b,d): $\Omega = 3.4$. Other parameters are the same as in Fig. 9. L is the locking ratio which measures the value of spiking frequency divided by the HFS frequency.

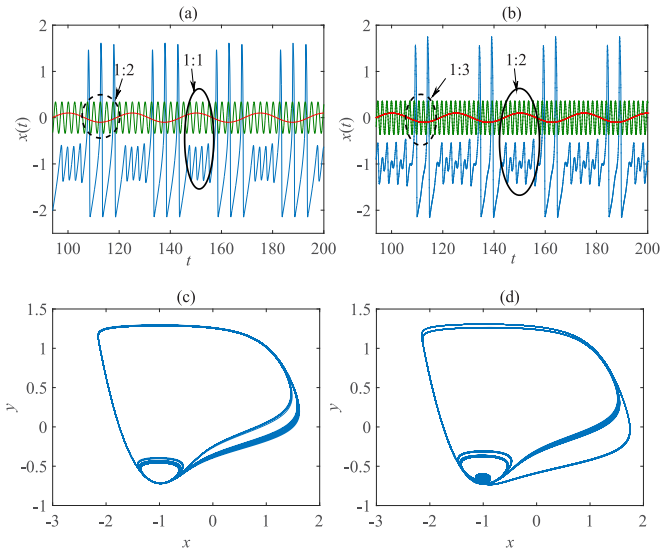

FIG. 11. (a–b) Time series of $x(t)$ (blue), LFS (red), and HFS (green). Dashed (solid) circles exhibit the locking ratios between the spikes (the subthreshold oscillations) and the HFS. (c,d) Phase portraits corresponding to (a,b). Parameters: (a,c) $B = 0.017$, $\Omega = 2.51$; (b,d) $B = 0.119$, $\Omega = 3.52$. Other parameters are in the text. The amplitudes of LFS and HFS have been magnified for a better view.

we name the phase locking in Fig. 9 or Fig. 10 as m:n suprathreshold phase locking). It is interesting that despite the fact $\Omega = 3.5$ is not the multiple of subthreshold oscillation frequency, the subthreshold oscillation is "adjusted" by making a small oscillation between two relatively larger oscillations [please compare Figs. 11(c) and 11(d)]. As a consequence, 1:2 subthreshold phase locking is found [see Figs. 11(b) and 11(d)]. Through the above analysis, the two maxima of response amplitude Q_{th} can be explained by two kinds of phase locking, namely, subthreshold and suprathreshold phase locking. We have also verified situations for $a = 1.01$ and other values of w, e.g., $w = 0.1$, which showed similar results. It should be noted that in spite of the different natures of $a = 1.01$ and 0.998 in the subthreshold case, the suprathreshold case for them showed no qualitative distinction.

IV. CONCLUSIONS AND DISCUSSIONS

In conclusion, we have studied the subthreshold and suprathreshold VR in the FitzHugh-Nagumo neuron model theoretically and numerically. For the subthreshold VR, two different cases were considered, namely, $a = 1.01$ and $a = 0.998$. They showed different features for both large frequencies (much larger than the canard-resonance frequency) and small frequencies (near the canard-resonance frequency) of HFS. When Ω is much larger than the canard-resonance frequency, the general trend of the response amplitude Q for both cases is that Q decreases with the increase of the HFS amplitude B and as the HFS frequency decreases the decreasing rate increases. But in detail, nonmonotonic decrease for case 2 was found with the periodiclike enhancement and attenuation of the response to LFS, in contrast to the monotonic decrease for case 1. Yet, due to the tiny value of the response amplitude Q, it remains to be validated whether it is possible to find these changes and the differences between the two cases experimentally. When Ω is near the canard-resonance frequency, the typical bell-shaped forms demonstrate the VR phenomenon, whereas for case 1, there is only one peak but for case 2, there are two. The results can be verified by the width of the orbit of x in Fig. 4 and the phase portraits in Fig. 5 (or Fig. 7). Moreover, although subthreshold oscillation is not important in information transmission [18], subthreshold VR does enhance the neuron firing behavior at the presence of noise which is demonstrated by the well pronounced peaks of the firing rate. Especially in neuronal networks, the authors have found the nontrivial phenomenon induced by the distance-dependent delay [27], so it would be of great interest to investigate the interplay between subthreshold VR and inevitable delay in different types of network topologies.

For the suprathreshold VR, we verified that the maxima of response amplitude Q_{th} of the FHN neuron model with HFS and LFS added to the slow variable y were still located at the transition boundaries of phase-locking patterns, as was compared with the fast variable situation in Ref. [8]. However, it was found that two local minimal required forcing amplitudes B of the firing onset were located at $\Omega = 2.5$ and 3.75, as a result of the frequency matching between the spiking frequency (around 1.25) and HFS frequency (multiples of 1.25). We predict other multiples of spiking frequency, e.g., 1.25 and 5, could also induce local minimal required forcing amplitude B of the firing onset. Furthermore, it was found that the two maxima of Q at $\Omega = 2.5$ and 3.5 were achieved by two kinds of phase locking: subthreshold and suprathreshold phase locking.

The focus on vibrational resonance has long been not only of mathematical interest but also of practical value, especially in neuroscience. Previous studies were mostly devoted to the single parameter of HFS, mainly to the amplitude. Global views of both amplitude and frequency of HFS on VR were seldom investigated. It has been verified that the frequency of LFS also has significant impacts on the quantic oscillator with monostable potentials [11]; thus it deserves future work to investigate the combined influence of amplitude and frequency of LFS, or in other words, VR's selectivity to LFS (which LFS is most enhanced by the system?). Besides, since neurons exist *in vivo* in the form of clusters, it is of practical significance to do research on VR in neuronal networks [28,29] and its roles in propagation [12,30]. In this paper, it is found that subthreshold VR can improve the firing rate at the presence of noise, so it could be anticipated that subthreshold VR may also enhance synchronization and propagation in neuronal networks.

ACKNOWLEDGMENTS

This research was supported by the National Natural Science Foundation of China (Grants No. 11472126 and No. 11232007) and the Project Funded by the Priority Academic Program Development of Jiangsu Higher Education Institutions (PAPD).

[1] R. Benzi, A. Sutera, and A. Vulpiani, J. Phys. A **14**, L453 (1981).
[2] L. Gammaitoni, P. Hanggi, P. Jung, and F. Marchesoni, Rev. Mod. Phys. **70**, 223 (1998).
[3] Z. Danziger and W. M. Grill, J. Comput. Neurosci. **38**, 53 (2015).
[4] S. Zambrano, J. M. Casado, and M. A. F. Sanjuán, Phys. Lett. A **366**, 428 (2007).
[5] J. P. Baltanas, L. Lopez, I. I. Blechman, P. S. Landa, A. Zaikin, J. Kurths, and M. A. F. Sanjuan, Phys. Rev. E **67**, 066119 (2003).
[6] P. S. Landa and P. V. E. McClintock, J. Phys. A **33**, L433 (2000).
[7] B. Deng, J. Wang, X. Wei, H. Yu, and H. Li, Phys. Rev. E **89**, 062916 (2014).
[8] L. Yang, W. Liu, M. Yi, C. Wang, Q. Zhu, X. Zhan, and Y. Jia, Phys. Rev. E **86**, 016209 (2012).
[9] C. Yao, Y. Liu, and M. Zhan, Phys. Rev. E **83**, 061122 (2011).
[10] C. Jeevarathinam, S. Rajasekar, and M. A. F. Sanjuan, Phys. Rev. E **83**, 066205 (2011).
[11] S. Jeyakumari, V. Chinnathambi, S. Rajasekar, and M. A. F. Sanjuan, Phys. Rev. E **80**, 046608 (2009).
[12] E. Ullner, A. Zaikin, J. Garcia-Ojalvo, R. Bascones, and J. Kurths, Phys. Lett. A **312**, 348 (2003).
[13] R. Fitzhugh, Biophys. J. **1**, 445 (1961).
[14] S. Khosrovani, R. S. Van der Giessen, C. I. De Zeeuw, and M. T. G. De Jeu, Proc. Natl. Acad. Sci. USA **104**, 15911 (2007).
[15] R. Amir, M. Michaelis, and M. Devor, J. Neurosci. **22**, 1187 (2002).
[16] D. Schmitz, T. Gloveli, J. Behr, T. Dugladze, and U. Heinemann, Neuroscience **85**, 999 (1998).
[17] C. N. Liu, M. Michaelis, R. Amir, and M. Devor, Journal of Neurophysiology **84**, 205 (2000).
[18] E. I. Volkov, E. Ullner, A. A. Zaikin, and J. Kurths, Phys. Rev. E **68**, 026214 (2003).
[19] B. Sancristobal, J. M. Sancho, and J. Garcia-Ojalvo, Phys. Rev. E **82**, 041908 (2010).
[20] V. A. Makarov, V. I. Nekorkin, and M. G. Velarde, Phys. Rev. Lett. **86**, 3431 (2001).
[21] M. A. Zaks, X. Sailer, L. Schimanskygeier, and A. B. Neiman, Chaos **15**, 026117 (2005).
[22] J. H. Yang and X. B. Liu, J. Phys. A **43**, 122001 (2010).
[23] J. H. Yang and X. B. Liu, Chaos **20**, 033124 (2010).
[24] D. L. Hu, J. H. Yang, and X. B. Liu, Comput. Biol. Med. **45**, 80 (2014).
[25] D. Hu, J. Yang, and X. Liu, Commun. Nonlinear Sci. Numer. Simul. **17**, 1031 (2012).
[26] B. Lindner, J. Garcia-Ojalvo, A. Neiman, and L. Schimansky-Geier, Phys. Rep. **392**, 321 (2004).
[27] J. Zhu, Z. Chen, and X. Liu, Phys. Rev. E **93**, 042417 (2016).
[28] B. Deng, J. Wang, X. Wei, K. M. Tsang, and W. L. Chan, Chaos **20**, 013113 (2010).
[29] Y. Haitao, G. Xinmeng, W. Jiang, D. Bin, and W. Xile, Physica A **436**, 170 (2015).
[30] R. Jothimurugan, K. Thamilmaran, S. Rajasekar, and M. A. F. Sanjuan, Int. J. Bifurcation Chaos **23**, 1350189 (2013).